Electronic Supplementary Material (ESI) for Physical Chemistry Chemical Physics.

Solvation Structure and Energetics of Electrolytes for Multivalent Energy Storage

Saul H. Lapidus,[a,§] Nav Nidhi Rajput,[b,§] Xiaohui Qu,[b] Karena W. Chapman,[a,*] Kristin A. Persson,[b,*] Peter J. Chupas[a,*]

[a] X-ray Science Division, Advanced Photon Source, Argonne National Laboratory, Argonne, Illinois, 60439, USA

[b] Environmental Energy Technology Division, Lawrence Berkeley National Laboratory, Berkeley, California 94720, USA

§ *These authors contributed equally*

Supporting Information

* Author to whom correspondence should be addressed:

chupas@aps.anl.gov; KAPersson@lbl.gov; chapmank@aps.anl.gov

X-ray Scattering Measurements

Solutions of 0.4 M $A(TFSI)_{1 \text{ or } 2}$ in diglyme ($A^{+/2+}$ = Li^+; Na^+; K^+; Mg^{2+}; Ca^{2+}; Zn^{2+}) were prepared in a glove box. This concentration was selected as a lower bound for practical battery applications with concentrations up to ~1 M typical of Li batteries.[1] Anhydrous diglyme was used as received from Sigma Aldrich. X-ray total scattering data were measured at beamline 11-ID-B at the Advanced Photon Source at Argonne National Laboratory utilizing high energy X-rays and a Perkin Elmer area detector. The 2D images were reduced to 1-D scattering data within fit2d. The data were corrected for background, Compton scattering, and oblique incidence effects and Fourier transformed to give pair distribution functions (PDFs) within pdfgetX2. A Lorch function was applied to minimize the impact of Fourier truncation ripples on the subsequent analysis.

To evaluate the impact of adventitious water on the data, a series of $Mg(TFSI)_2$/diglyme solutions were studied, for which increasing amounts of added water (Figure S1). The data show large changes with added water, with little similarity of the water-associated features and the data for the anhydrous solution, suggesting minimal water existed in the original solutions.

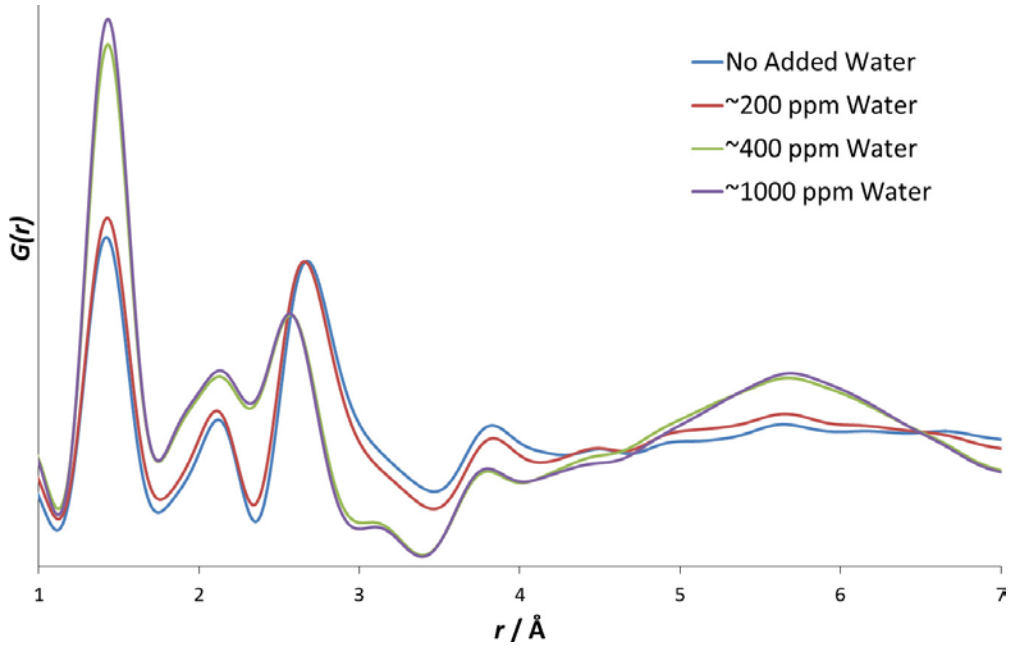

Figure S1. Small quantities of water added to the $Mg(TFSI)_2$/diglyme solution induces pronounced changes to the PDF data, suggesting that the original solution is effectively anhydrous.

Principal Component Analysis

Principal component analysis (PCA) was performed within Origin 9.1. The PDFs for LiTFSI and $Zn(TFSI)_2$ were excluded from the data used to derive the principal component and, thus, serve as an independent verification of the analysis. The data analyzed correspond to solutions of equal concentration, thereby eliminating the impact of possible concentration-dependent phenomena. In principle, variable concentration studies could be applied to explore concentration effects and to separate any well-defined solvent-anion and anion-anion correlations. Both the eigenvalues and eigenvectors were evaluated. In the present series, in which the cation alone was varied, only the first component, which corresponds to *intra*-molecular TFSI distances and *inter*-molecular TFSI-diglyme distances has physical relevance. This is supported by the eigenvalues, which indicate that all of the PDFs have a similar relative contribution from this principal component.

Subsequent differential analysis, subtracting the common first/principal component from the total PDFs was applied to recover the *d*-PDFs corresponding to the cation solvation environment. For each PDF, the principal component was scaled to minimize features below ~1.5 Å which are exclusive to intra-molecular correlations. The similarity of features in the *d*-PDFs for Li and Zn (which were not included in the PCA) suggests that the principal component provides a reliable measure of the *intra*-molecular TFSI distances and *inter*-molecular TFSI-diglyme distances.

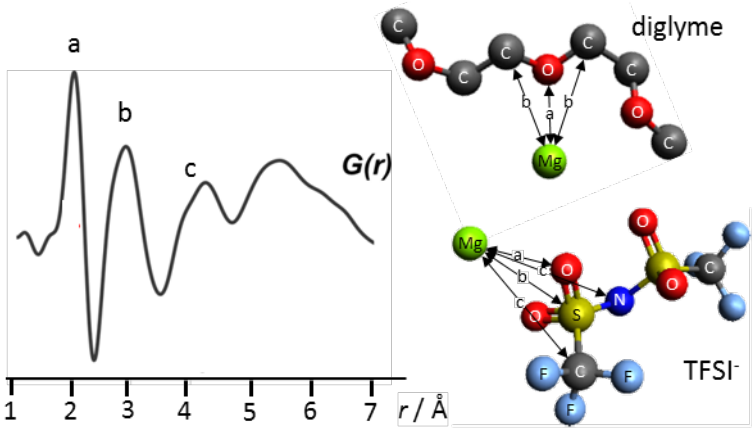

Figure S2: A schematic illustrating the likely Mg…X distances corresponding to features in the d-PDF

Modeling

Molecular dynamics simulations were performed to understand the solvation structure of Mg-TFSI in diglyme. The simulations were undertaken using the Gromacs MD simulation package version 4.5.3.[2] The force field parameters evaluated for Mg are listed in Table 1S include the AMBER force field by Aqvist[3-4], the OPLSAA force field by Jorgensen[5] and the force field developed by Callahan[6]. The force field for TFSI was taken from Kelkar and Maginn.[7] The force field for diglyme was developed by obtaining the partial charges from electronic structure calculations and taking the force field parameters from a generalized amber force field (GAFF).[8] Figure S3 shows the radial distribution function of $Mg(TFSI)_2$ in diglyme using different force fields studied in this work. The peak ~ 2.1 Å is observed for Mg-O(TFSI) and Mg-O (diglyme) and at ~ 4 Å for Mg-N(TFSI). A difference of ~0.4 Å is observed in the peak position of Mg-O and Mg-N(TFSI) using different force fields. The RDF obtained using OPLSAA force field are in very good agreement with the experimental PDF results. The Mg-O distance in Aqvist is shorter by ~ 0.2 Å and is greater by ~0.2 Å in Callahan force field than the experimental result (red and blue curves in Fig. S3 (a) and (b)). Slight changes in the force field parameters of Mg^{2+} produced significant changes in the RDF. Energy minimization was performed to relax the strained contacts in the initial configuration using steepest descent and then conjugate gradient. The simulations were performed in an isothermal-isobaric ensemble (constant *NPT*) ensemble for 2 ns followed by 5 ns production runs in canonical ensemble (constant *NVT*) ensemble at 298 K. The improved velocity-rescaling algorithm proposed by Parrinello *et al*. was used to maintain the temperature at 298 K with a time constant of 0.1 ps. The particle-mesh Ewald (PME) method with a cut-off distance of 1.2 nm was used to handle the long-range electrostatic interactions and Lenard-Jones interactions were truncated at a distance of 1.0 nm. Periodic boundary conditions were implied in XYZ directions. The size of the simulation box was approximately 40 x 40 x 40 Å. Results were averaged over two independent configurations of the same system.

TABLE S1. Simulation Parameters for Mg^{2+}

	q (e)	**α (Å³)**	**r (Å)**	**ε (kcal/mol)**
Aqvist/ff994	+2	0.120	0.7926	0.8947
OPLSAA	+2	0.000	0.9929	0.8750
Callahan	+2	0.000	1.0600	0.8750

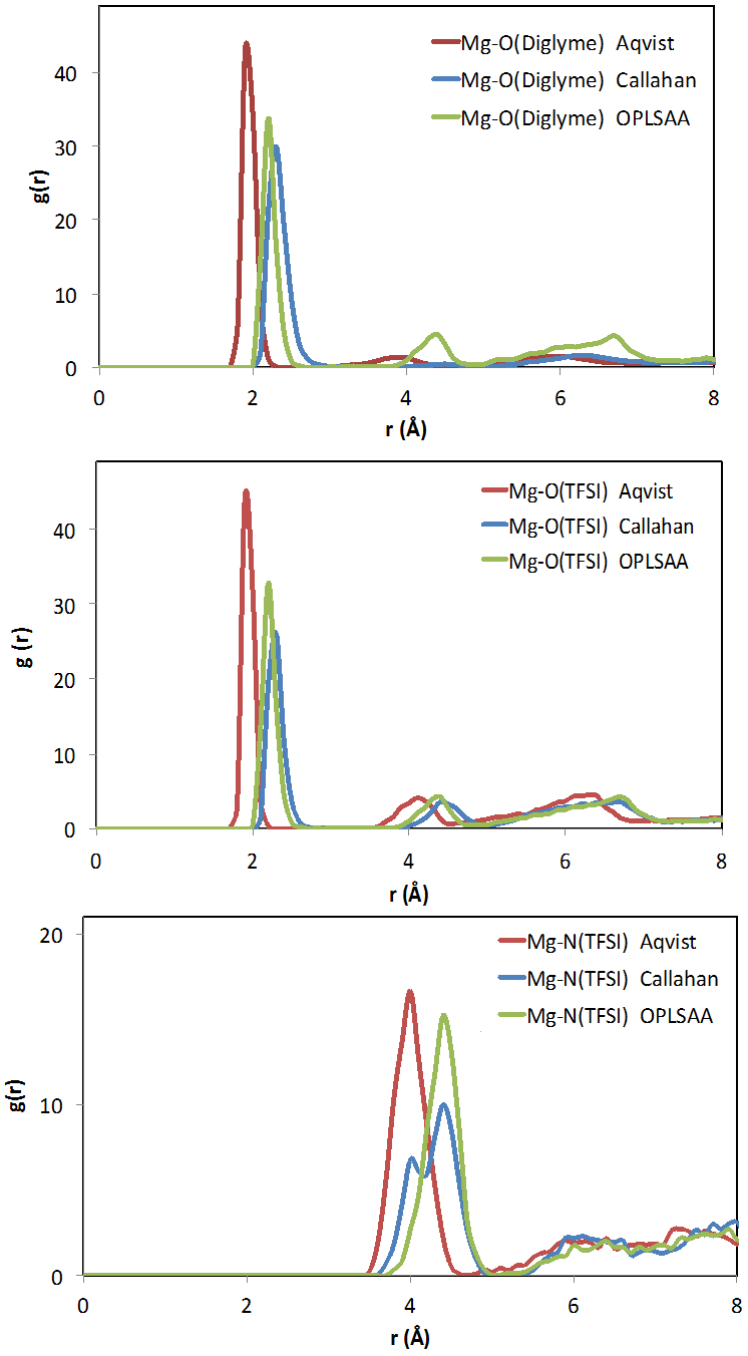

Figure S3. The RDFs of Mg-O(diglyme), Mg-O(TFSI) and Mg-N(TFSI) for the different force fields of Mg^{2+} presented in Table S1.

The desolvation energy was evaluated using the dissociative mechanism. It employs classical MD simulations to predict the solvation structure and Density Functional Theory (DFT) to compute the energy penalty in removing solvents from the solvation shells of ions. [9] From the MD simulations 4 different snapshots were taken capturing the first solvation shell around Mg^{2+}. The snapshots were selected according to the coordination number of TFSI and diglyme in the first solvation shell of Mg^{2+}. The snapshots were used as the starting point for the DFT potential energy surface scan, which is expected to manifest the energy in removing the first solvation shell. The potential energy surface scan was carried out by a series of constrained geometry optimizations at the B3LYP/6-31+G(d) level. The Mg…O bond length is fixed in every geometry optimization and used as the reaction coordinate. To reveal the energy barrier of first solvation shell elimination, the Mg…O bond is stretched up to 3.7 Å. The QChem software package was employed to perform the DFT calculations. [10] An implicit solvent model SM12-MK was also used to corroborate the desolvation energy calculated from dissociative mechanism.[11]

Figure S4 shows the energy scan for dissociation of diglyme from $Mg(TFSI)_2$ for 4 different snapshots (SS1-SS4) taken from MD simulations. Dissociating diglymes from the first solvation shell resulted in an average energy barrier of ~ 17.36 kcal/mol. The energy barrier observed for Mg^{2+} without $TFSI^-$ is ~ 33.67 kcal/mol. This higher energy barrier suggest that $TFSI^-$ enhances the solvation of $Mg(TFSI)_2$ in diglyme.

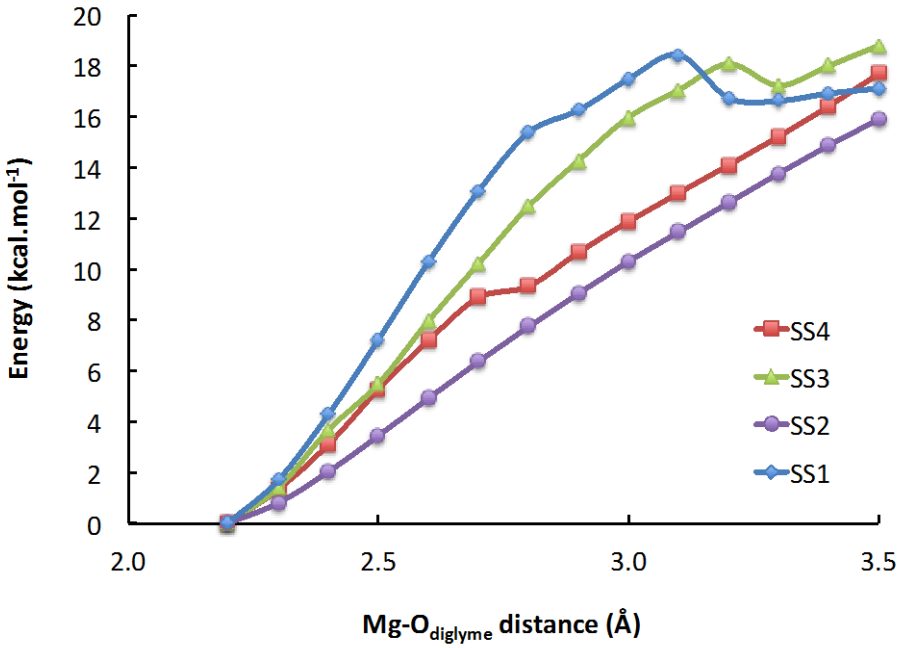

Figure S4. Energy scan profile along the diglyme dissociation with Mg (TFSI)$_2$

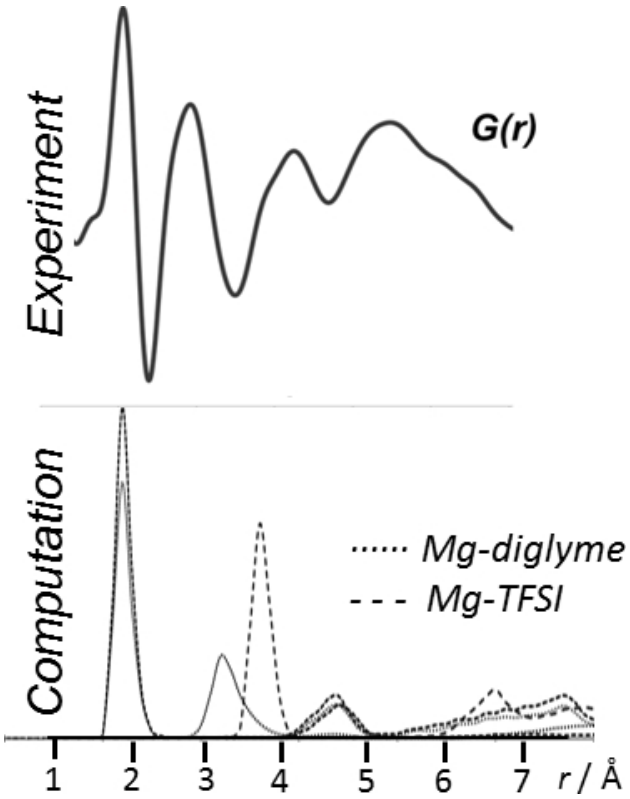

Figure S5. A comparison of the experimental d-PDF (G(r), top) and the computational RDF (g(r), bottom).

References

1. D. Aurbach, *Nonaqueous electrochemistry*, CRC Press, 2002.
2. S. Pronk, S. Páll, R. Schulz, P. Larsson, P. Bjelkmar, R. Apostolov, M. R. Shirts, J. C. Smith, P. M. Kasson and D. van der Spoel, *Bioinformatics*, 2013, btt055.
3. J. Aaqvist, *J. Phys. Chem.*, 1990, **94**, 8021-8024.
4. W. D. Cornell, P. Cieplak, C. I. Bayly, I. R. Gould, K. M. Merz, D. M. Ferguson, D. C. Spellmeyer, T. Fox, J. W. Caldwell and P. A. Kollman, *Journal of the American Chemical Society*, 1995, **117**, 5179-5197.
5. W. L. Jorgensen, *Yale University: New Haven, CT*, 1997.
6. K. M. Callahan, N. N. Casillas-Ituarte, M. Roeselová, H. C. Allen and D. J. Tobias, *J. Phys. Chem. A*, 2010, **114**, 5141-5148.
7. M. S. Kelkar and E. J. Maginn, *J. Phys. Chem. B*, 2007, **111**, 4867-4876.
8. J. Wang, R. M. Wolf, J. W. Caldwell, P. A. Kollman and D. A. Case, *Journal of computational chemistry*, 2004, **25**, 1157-1174.
9. Y. Yang, N. Sahai, C. S. Romanek and S. Chakraborty, *Geochim. Cosmochim. Acta*, 2012, **88**, 77-87.
10. s. h. w. Development version of the Q-Chem program package and q-chem.com.
11. A. V. Marenich, C. J. Cramer and D. G. Truhlar, *J. Chem. Theory Comput.*, 2012, **9**, 609-620.